Original Article

Institution of MECHANICAL ENGINEERS

Journal of AEROSPACE ENGINEERING

Proc IMechE Part G:
J Aerospace Engineering
0(0) 1–11

DOI: 10.1177/0954410016636157
uk.sagepub.com/jaero
SAGE

Analysis of a mechanism with redundant drive for antenna pointing

Xin Li[1,2], Xilun Ding[1] and Gregory S Chirikjian[2]

Abstract

Orientation accuracy is a key factor in the design of mechanisms for antenna pointing. Our design uses a redundantly actuated parallel mechanism which may provide an effective way to solve this problem, and even can increase its payload capability and reliability. The presented mechanism can be driven by rotary motors fixed on the base to reduce the inertia of the moving parts and to lower the power consumption. The mechanism is redundantly actuated by three arms, and is used as a two-dimensional antenna tracking and pointing device. Both the forward and inverse kinematics are investigated to find all the possible solutions. Detailed characters of the platform are analyzed to demonstrate the advantages in eliminating singularities and improving pointing accuracy. A method of calculating the overconstrained orientational error is also proposed based on the differential kinematics. All the methods are verified by numerical examples.

Keywords

Antenna pointing mechanism, redundant drive, orientation workspace, singularity analysis, error analysis

Date received: 14 April 2015; accepted: 27 January 2016

Introduction

Conventional antenna mounts are serial kinematic devices with floating actuators as a part of the moving platform. The floating actuators lead to extra weight and rotary inertia. In order to lower the power consumption and improve the mobility, all of the actuators should be fixed to the base. Moreover, while a typical parallel mechanism consisting of more sub-chains can improve the accuracy and the load capacity of its platform. A two degrees of freedom (DOF) parallel antenna, named the Canterbury tracker, together with an analysis of its kinematics, has been studied by Dunlop and Jones.[1] Two actuated arms, one passive arm, and a strut, are attached to the platform and the base. The movable strut is not good for higher load capacity, but it is a novel design method. The antenna pointing device is actually a two or three DOF rotational mechanism. Accordingly, the relevant studies are investigated.

The well-known Omni-Wrist III is another two-DOF parallel mechanism. Driven by two linear actuators, it is capable of a full hemisphere of pitch/yaw motion.[2] Two-DOF parallel wrists with two rotary motors have been presented by Carricato and Parenti-Castelli,[3] and Gogu,[4] respectively. The workspace and the kinematics of one type of the wrist mechanisms have been studied,[5] and the singularities have been analyzed by using a visual graphic approach.[6] Merriam et al.[7] developed a fully compliant pointing mechanism to eliminate friction and the joint backlash, but further design is needed to increase the workspace volume. For several reasons, more actuators than the number of DOF are often used. A redundantly actuated mini pointing device was described by Palpacelli, et al.[8] To increase the workspace size of this flexure-base mechanism, a redundant linear actuator was added. Shao et al.[9] designed a tilt platform driven by three piezoelectric actuators. Saglia et al.[10] presented a high performance ankle rehabilitation mechanism. Driven by three linear actuators, the mechanism could deliver enough forces and torques needed for ankle exercises. Similar platforms include another three-DOF ankle rehabilitation mechanism proposed by Wang, et al.[11] A spherical wrist was proposed to show that actuator redundancy not only removed singularities but also increased dexterity.[12] Some singularity-free spherical wrists with parallel structure have been addressed by Lenarcic and Stanisic[13] and Enferadi and

[1]School of Mechanical Engineering & Automation, Beihang University, Beijing, China
[2]Department of Mechanical Engineering, Johns Hopkins University, Baltimore, USA

Corresponding author:
Gregory S Chirikjian, Department of Mechanical Engineering, Johns Hopkins University, 3400 N. Charles Street, Baltimore 21218, USA.
Email: gchirik1@jhu.edu

Tootoonchi,[14] respectively. To simulate the humanoid humeral pointing motion, a parallel platform with moveable central strut was designed.[15–17] Di Gregorio[18] presented a family of three legs parallel spherical mechanisms. They are all spherical parallel mechanisms with many common characteristics, such as the kinematic properties including the singularity problems.[19,20]

For the antenna pointing mechanism structure design, this paper proposes a rotational parallel platform with 2-DOF which is redundantly driven by three rotary motors. A central strut is used to improve the load capacity. The solutions are analyzed for both the forward and inverse kinematics. Then the workspace and the singularity analysis are presented. Furthermore, the pointing errors caused by joint clearances in redundant and non-redundant situations both are studied. The presented platform can also be used as mechanical eyes, robot wrists, and rehabilitation devices, etc.

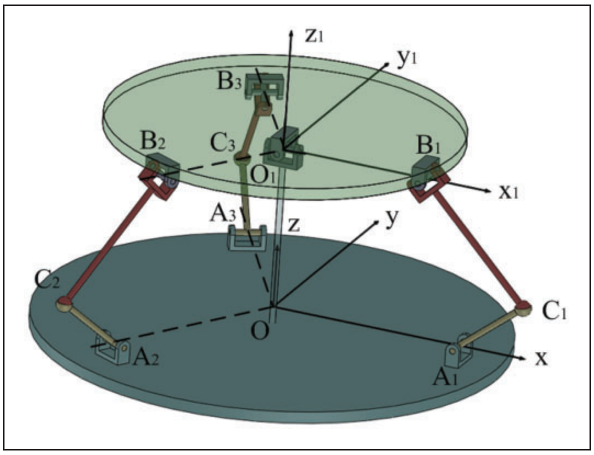

Figure 1. A 2-DOF rotary parallel mechanism.

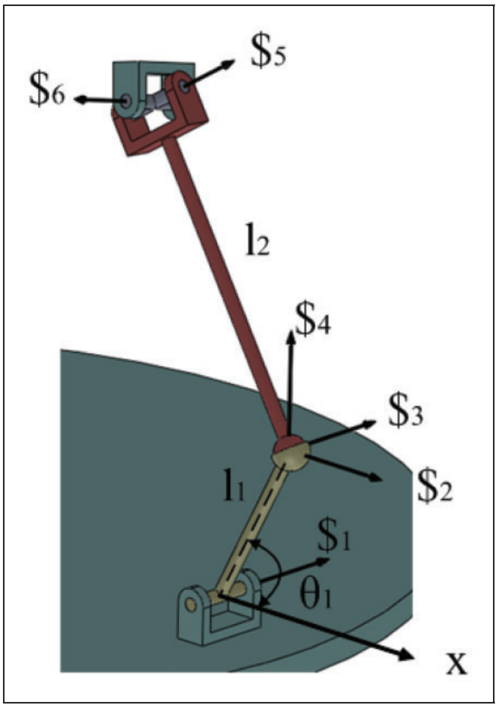

Figure 2. Kinematic description of the R-S-U arm.

Kinematics solution

Forward and inverse kinematics

A parallel pointing mechanism with three arms is presented as shown in Figure 1. It consists of a platform and a base. They are connected by a central strut and three identical arms. The central strut is fixed at the center of the base, and the other end is connected to the centroid of the upper platform by a universal joint. Arm1 ($A_1C_1B_1$) with three joints is as shown in Figure 2. The revolute joints of the three arms are uniformly placed around the periphery of the base (marked as A), while the three universal joints are placed uniformly around the periphery of the upper platform (marked as B). Two parts of each arm are connected by a spherical joint (marked as C). Let the upper platform surface be parallel to the base surface, and it is as the initial (home) position of this mechanism. Point $\boldsymbol{O}$ is located at the centroid of points $\boldsymbol{A}_1$, $\boldsymbol{A}_2$, and $\boldsymbol{A}_3$, while point $\boldsymbol{O}_1$ is located at the centroid of points $\boldsymbol{B}_1$, $\boldsymbol{B}_2$, and $\boldsymbol{B}_3$. In Figures 1 and 2, coordinates $\boldsymbol{O}$-xyz and $\boldsymbol{O}_1$-$x_1y_1z_1$ are affixed to the base and the upper platform, respectively, with their z-axes point vertically upwards. Axis x is along line OA_1, and axis x_1 is along line O_1B_1. They are parallel lines at the initial position, and axis y_1 coincides with the floating axis of the central strut universal joint. In Figure 1, the height of OO_1 is h; Lengths of OA_i, O_1B_i, A_iC_i, and C_iB_i $(i = 1, 2, 3)$ are R, r, l_1, and l_2, respectively.

The central universal joint is as shown in Figure 3. The fixed coordinate $\boldsymbol{O}_1$-$x_{10}y_{10}z_{10}$ is parallel to the base surface, and it is the initial state of $\boldsymbol{O}_1$-$x_1y_1z_1$.

Furthermore, the parallel platform can be proved as a 2-DOF rotational mechanism. If any two revolution joints of the three arms are driven by actuators, the platform is fully constrained. Accordingly, the motions can be controlled by two fixed rotary motors. If driven by three arms, the mechanism is redundantly actuated, which will be focused on in this paper. Also, if the universal joint of the central strut is replaced by a spherical joint, the platform turns into a 3-DOF rotational device which can also be applied as an antenna pointing mechanism.

The forward kinematics for this mechanism involves determining the angular position, velocity, and acceleration of the upper platform by giving the driven arm angles, while the inverse kinematics is the reverse process. In Figure 1, arms $A_1C_1B_1$, $A_2C_2B_2$, and $A_3C_3B_3$ can be called arm1, arm2, and arm3 and let their position angles be θ_1, θ_2, and θ_3, respectively.

Every point at the upper platform can be determined by performing two rotations. In Figure 3, the

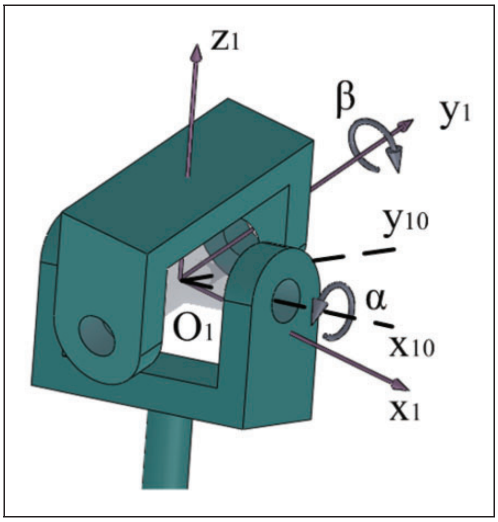

Figure 3. Universal joint of central strut.

platform first rotates α about axis x_1, and then rotates β about the axis y_1. $\mathbf{R}_x$ denotes the first rotation matrix, and then the direction of the floating axis y_1 is

$$\boldsymbol{y}_1 = \mathbf{R}_x \boldsymbol{y}_{10} = \begin{bmatrix} 1 & 0 & 0 \\ 0 & c\alpha & -s\alpha \\ 0 & s\alpha & c\alpha \end{bmatrix} \begin{bmatrix} 0 \\ 1 \\ 0 \end{bmatrix} = \begin{bmatrix} 0 \\ c\alpha \\ s\alpha \end{bmatrix} \tag{1}$$

where c and s denote cos and sin, respectively.

Let the rotation matrix about y_1 be $\mathbf{R}_{y1}$, and

$$\mathbf{R}_{y1} = \begin{bmatrix} c\beta & -s\alpha s\beta & c\alpha s\beta \\ s\alpha s\beta & c^2\alpha + s^2\alpha c\beta & s\alpha c\alpha(1-c\beta) \\ -c\alpha s\beta & s\alpha c\alpha(1-c\beta) & s^2\alpha + c^2\alpha c\beta \end{bmatrix} \tag{2}$$

In the base coordinate, point $\boldsymbol{B}_i$ (i = 1, 2, 3) can be obtained by using matrix multiplication

$$\boldsymbol{B}_i = \boldsymbol{O}_1 + \mathbf{R}_{y1}\mathbf{R}_x \boldsymbol{B}_{i0}, \quad (i = 1, 2, 3) \tag{3}$$

where $\boldsymbol{B}_{i0}$ is the initial position vector (3×1).

According to the structure constraint

$$\|\boldsymbol{B}_i - \boldsymbol{C}_i\| = l_2, \quad (i = 1, 2, 3) \tag{4}$$

three equations are obtained for the arms

$$F_i = p_{i1} s\theta_i + p_{i2} c\theta_i + p_{i3} = 0 \tag{5}$$

where, p_{ij} are the corresponding dimensional parameters.

According to equation (5), F_i is a function of α, β, and θ_i, so the solution of the inverse kinematics is easy to get.

Table 1. Structure parameters (*mm*).

R	r	h	l_1	l_2
166	126	140	70	134

Let

$$t_i = \tan\frac{\theta_i}{2} \tag{6}$$

then

$$t_i = \frac{-p_{i1} \pm \sqrt{\Delta_i}}{(p_{i3} - p_{i2})}, \quad \Delta_i = p_{i1}^2 + p_{i2}^2 - p_{i3}^2 \tag{7}$$

Thus, the displacement of each arm is obtained.

The forward kinematics of parallel mechanisms is a challenging problem.[21] For the forward kinematics of this two-DOF mechanism, only two of the three arms are needed to determine the rotation angles of the platform, even all of the three arms are actively driven. Taking arm1 and arm2 as active sub-chains, variables α and β can be determined by θ_1 and θ_2. Rearrange (5) as

$$F_1 = q_{11} c\beta + q_{12}\, c\,\alpha\, s\beta + q_{13} = 0 \tag{8}$$

where

$$\begin{cases} q_{11} = -2r(R + l_1 c\theta_1) \\ q_{12} = 2r(-h + l_1 s\theta_1) \\ q_{13} = R^2 + r^2 + h^2 + l_1^2 - l_2^2 - 2l_1(hs\theta_1 - Rc\theta_1) \end{cases} \tag{9}$$

Similarly, let

$$t_\alpha = \tan\frac{\alpha}{2}, \quad t_\beta = \tan\frac{\beta}{2} \tag{10}$$

Solving the resulting quadratic equation for t_β gives

$$t_\beta = \frac{q_{12}(t_\alpha^2 - 1) \pm \sqrt{\Delta_{\alpha 1}}}{(q_{13} - q_{12})(t_\alpha^2 + 1)}, \quad \Delta_{\alpha 1} = (q_{11}^2 - q_{13}^2) \times (t_\alpha^2 + 1)^2 + q_{12}^2(t_\alpha^2 - 1)^2 \tag{11}$$

The rotation angle β is then expressed as a function of α. Furthermore, it could be substituted into the equation for F_2 to get a closed-form solution. The solution is complicated and it is not an expected result. However, the explicit relationships between α and β according to equations F_1 and F_2 are given and it is important even a numerical method is used. A specific platform is constructed in Table 1 as an example.

The structure parameters of the proposed mechanism are listed in Table 1. Assume that θ_1 and θ_2 are at

30° and 60°, respectively. Repeating the process of equations (8) to (11) according to the result, the relationship of curves of α and β is as shown in Figure 4.

In Figure 4, two loops for arm1 and arm2 are drawn, respectively. As pointed in equation (11), there are two possible solutions, and in the figure, they are plotted in dashed lines and solid lines. The two intersection points of the loops are the possible solutions of the platform rotation angles. The two matched configurations are shown in Figure 5. The position of arm3 can be calculated from equation (7).

There are at most four intersections for two different loops. From the above analysis, it is known that by using equation (11), all possible solutions could be found even if the final forward kinematics closed-form solution is not given. In addition, as it is shown in Figure 4, the dashed line for arm1 is nearly parallel to axis α which means α is sensitive to β. So in equation (11), choosing the independent variable from t_α and t_β should be done carefully.

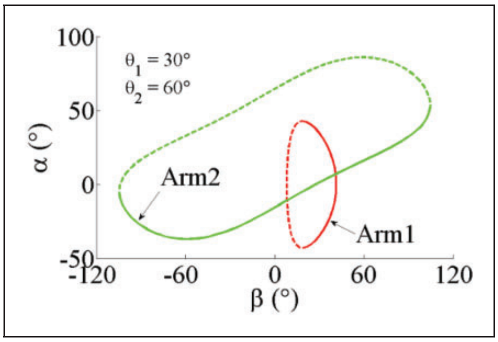

Figure 4. Curves for α and β.

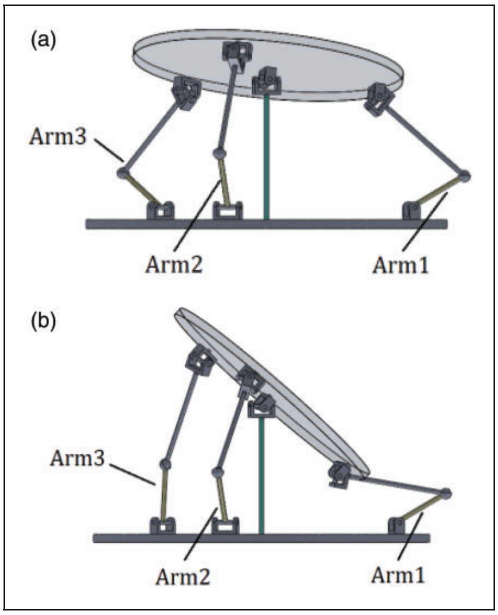

Figure 5. The two configurations of the forward kinematics solution. (a) Solution 1. (b) Solution 2.

The Jacobian matrix is establishes the relationship between the angular velocity of the upper platform and the active joint angular velocity. The partial derivative equations of equation (5) can be expressed as

$$J_{i\alpha}\dot{\alpha} + J_{i\beta}\dot{\beta} + J_{i\theta i}\dot{\theta}_i = 0 \tag{12}$$

where

$$\begin{cases} J_{1\alpha} = 2\mathrm{r}(h - l_1 s\theta_1)s\alpha s\beta \\ J_{1\beta} = 2\mathrm{r}[(R + l_1 c\theta_1)s\beta - (h - l_1 s\theta_1)c\alpha c\beta] \\ J_{1\theta 1} = 2l_1[(-h + rc\alpha s\beta)c\theta_1 - (R - rc\beta)s\theta_1] \end{cases} \tag{13}$$

$$\begin{cases} J_{2\alpha} = \mathrm{r}(-h + l_1 s\theta_2)\left(s\alpha s\beta + \sqrt{3}c\alpha\right) \\ \qquad + \frac{r}{2}(R + l_1 c\theta_2)\left(3s\alpha - \sqrt{3}c\alpha s\beta\right) \\ J_{2\beta} = \mathrm{r}(h - l_1 s\theta_2)c\alpha c\beta \\ \qquad + \frac{r}{2}(R + l_1 c\theta_2)\left(s\beta - \sqrt{3}s\alpha c\beta\right) \\ J_{2\theta 2} = l_1\left(-2h + \sqrt{3}rs\alpha - rc\alpha s\beta\right)c\theta_2 \\ \qquad - \frac{l_1}{2}\left(4R - \sqrt{3}rs\alpha s\beta - 3rc\alpha - rc\beta\right)s\theta_2 \end{cases} \tag{14}$$

$$\begin{cases} J_{3\alpha} = \mathrm{r}(-h + l_1 s\theta_3)\left(s\alpha s\beta + \sqrt{3}c\alpha\right) \\ \qquad + \frac{r}{2}(R + l_1 c\theta_3)\left(3s\alpha + \sqrt{3}c\alpha s\beta\right) \\ J_{3\beta} = \mathrm{r}(h - l_1 s\theta_3)c\alpha c\beta \\ \qquad + \frac{r}{2}(R + l_1 c\theta_3)\left(s\beta + \sqrt{3}s\alpha c\beta\right) \\ J_{3\theta 3} = l_1\left(-2h - \sqrt{3}rs\alpha - rc\alpha s\beta\right)c\theta_3 \\ \qquad - \frac{l_1}{2}\left(4R + \sqrt{3}rs\alpha s\beta - 3rc\alpha - rc\beta\right)s\theta_3 \end{cases} \tag{15}$$

The angular velocities of both forward and inverse kinematics can be accordingly obtained. Repeating the differentiate process, the angular accelerations can also be known.

Numerical example

A numerical example is calculated according to the derivation above. Taking the parameters as listed in Table 1, when α and β both move from−15° to 15° with constant speed 1°/s, the inverse displacements are shown in Figure 6.

According to equation (7), each arm has two possible inverse kinematics solutions. They are as shown in Figure 6(a) and (b), respectively. One set of the solutions is as shown in Figure 6(a), and the intersection point of the three lines indicates that the three arms have the same displacement at this moment. It matches the configuration in Figure 1 as the initial

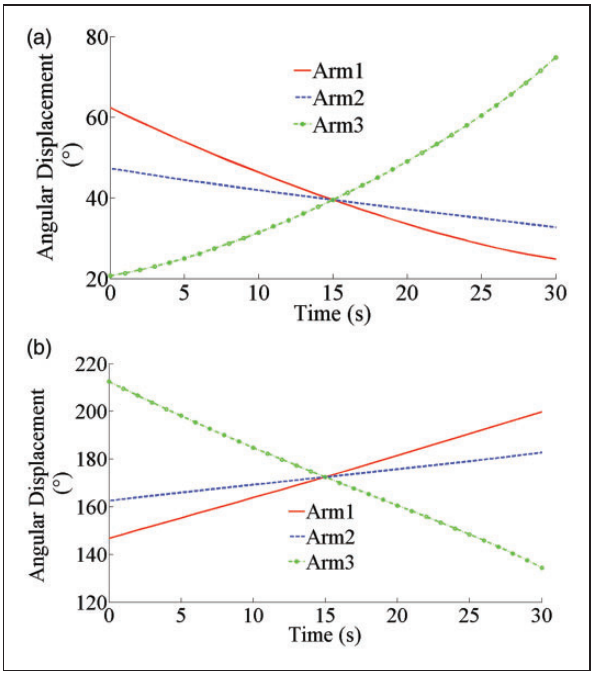

Figure 6. Angular displacements for the three arms. (a) Solution 1. (b) Solution 2.

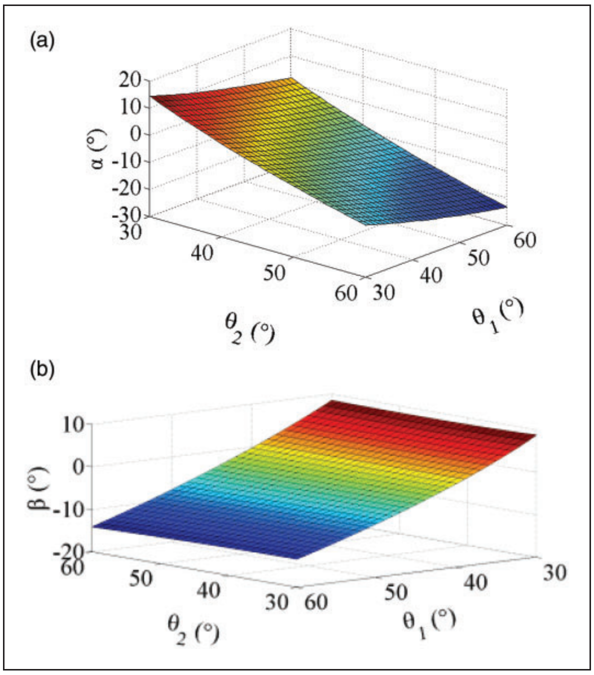

Figure 8. Displacement of α and β. (a) Displacement of α. (b) Displacement of β.

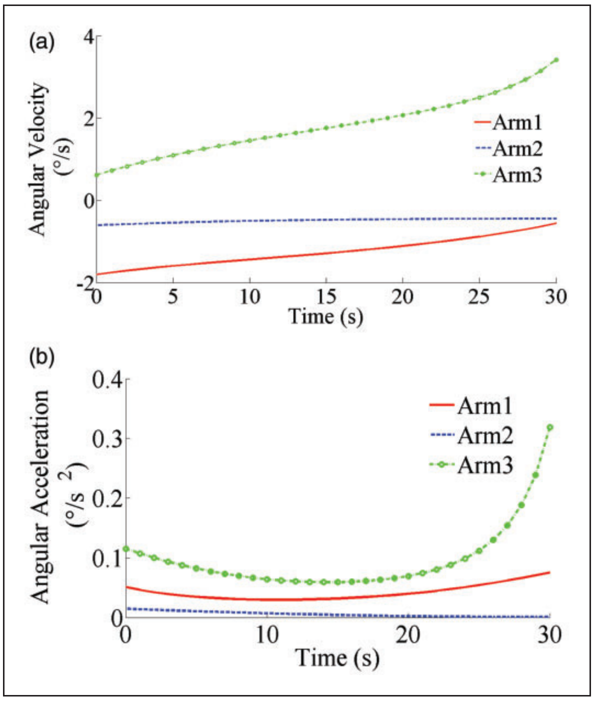

Figure 7. Angular velocities and accelerations for the three arms. (a) Angular velocities. (b) Angular accelerations.

position. In the configuration, the angular velocities and accelerations are given, as shown in Figure 7.

If the angular displacements of arm1 and arm2 both are from 30° to 60°, according to the forward kinematics analysis, the relationship between θ_1, θ_2, and α can be shown as a mesh in Figure 8(a). In the same way, another mesh can be obtained for β as shown in Figure 8(b).

Workspace and singularity

The workspace for the 2-DOF parallel mechanism considered as a pointing device is defined in the three-dimensional (3D) space, called orientation workspace. The orientation workspace is the set of all attainable orientations of the mobile platform about a fixed point. The 3D orientation workspace is nearly the most difficult one to represent.[22] The parallel mechanism closed-loop nature brings complex singularities inside the workspace. The singular configurations have an important influence on the performance of the parallel mechanisms. The problem has been addressed by using geometry method or by Jacobian matrix.[23–26] In addition, the redundantly actuated method has been applied to reduce or eliminate the singularities.[27]

In this section, the orientation workspace is analyzed with singularity configurations. Assuming that a unit vector from $\boldsymbol{O}_1$ pointing outwards is perpendicular to the upper platform surface. All the possible points which the end of the vector can attain constitute the workspace. Accordingly, in the coordinate system $\boldsymbol{O}_1$-$x_{10}y_{10}z_{10}$ as is shown in Figure 3, the orientation of the platform is

$$\boldsymbol{P} = \mathbf{R}_{y1}\mathbf{R}_x\begin{bmatrix}0 & 0 & 1\end{bmatrix}^T = \begin{bmatrix}s\beta & -s\alpha c\beta & c\alpha c\beta\end{bmatrix}^T \tag{16}$$

Searching all the values of α and β, if Δ_i in equation (7) are all greater or equal to zero, then α and β can be substituted in equation (16) to determine the workspace. Still using the parameters constructed in

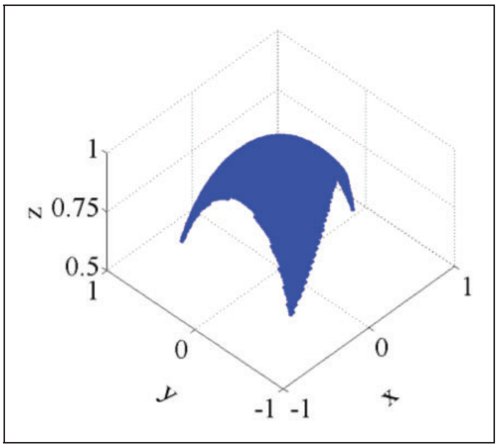

Figure 9. Orientation workspace.

Table 1, the workspace is as shown in Figure 9. In the figure, the orientation workspace is symmetric about axis x.

To identify the singularities in this workspace, the number and the locations of the actively arms should be known first. The reason is as follows.

Rearrange equation (12)

$$\begin{bmatrix} J_{1\alpha} & J_{1\beta} \\ J_{2\alpha} & J_{2\beta} \\ J_{3\alpha} & J_{3\beta} \end{bmatrix} \begin{bmatrix} \dot{\alpha} \\ \dot{\beta} \end{bmatrix} = - \begin{bmatrix} J_{1\theta 1} & 0 & 0 \\ 0 & J_{2\theta 2} & 0 \\ 0 & 0 & J_{3\theta 3} \end{bmatrix} \begin{bmatrix} \dot{\theta}_1 \\ \dot{\theta}_2 \\ \dot{\theta}_3 \end{bmatrix} \tag{17}$$

If the mechanism is driven by arm1 and arm2, and arm3 is passive, for the forward singularity

$$\begin{vmatrix} J_{1\alpha} & J_{1\beta} \\ J_{2\alpha} & J_{2\beta} \end{vmatrix} = 0 \tag{18}$$

Since θ_i can be expressed as a function of α and β, according to equations (6), (7), (13), and (14), the relationship between α and β in equation (18) is obtained. Then substituting the solved α and β in equation (16), all the singular points in the workspace can be determined. If arm2 or arm1 is passive, the singularity analysis is similar. Since each arm has two possible configurations, assuming the initial position of these arms is as shown in Figure 1, the top view of the orientation workspace discussed above with singularities is as shown in Figure 10.

In Figure 10, the dashed lines are where the mechanism is in singular configurations. In fact, the two lines A are singularities caused by arm1, and the lines B and C are caused by arm2 and arm3, respectively. From Figures 9 and 10, some characters of this mechanism can be known. In the coordinate system $\boldsymbol{O}_1$-$x_{10}y_{10}z_{10}$, the figure is only symmetrical about axis x_{10}, which means that even if the three arms are identical, the workspace will not be rotationally symmetric. The lines A in Figure 10(a) and (b) do not intersect the line B and the line C, so the singularities caused by arm1 can be totally eliminated by arm2 and arm3. To explain it, let

$$\begin{cases} \alpha = 22.9183^\circ \\ \beta = -12.7512^\circ \end{cases} \tag{19}$$

which fulfills equation (18) driven by arms 1 and 2, and this configuration is as shown in Figure 11.

It is difficult to identify which configurations in Figure 11(a) cause a singularity. So in Figure 11(b), it shows a geometric representation. Arm2 is represented by $A_2C_2B_2$. If only arm2 tries to control the platform, the instantaneous rotation axis can be determined as

$$\boldsymbol{s}_{a1} = [\,\mathrm{c}\alpha\mathrm{c}\beta - \mathrm{s}\beta\frac{R + l_1\mathrm{c}\theta_1}{h - l_1\mathrm{s}\theta_1} \quad \mathrm{c}\alpha\mathrm{s}\alpha\mathrm{s}\beta \quad \mathrm{s}^2\alpha\mathrm{s}\beta\,]^T \tag{20}$$

where from equations (6), (7), and (19) we get

$$\begin{cases} \theta_1 = 57.6163^\circ \\ \theta_2 = 19.4063^\circ \\ \theta_3 = 60.3638^\circ \end{cases} \tag{21}$$

So, the rotation axis in equation (20) is

$$\frac{\boldsymbol{s}_{a1}}{\|\boldsymbol{s}_{a1}\|} = [\,0.9983 \quad -0.0544 \quad -0.0230\,]^T \tag{22}$$

This axis has been plotted in Figure 11(b). As can be seen, the instantaneous rotation line intersects the extension line of C_2B_2. Arm2 cannot provide any drive torques, so the mechanism loses a degree of freedom.

To solve the forward singularity problem, use arm3 as an additional input, then

$$\begin{cases} \begin{vmatrix} J_{2\alpha} & J_{2\beta} \\ J_{3\alpha} & J_{3\beta} \end{vmatrix} \approx -9.7459 \times 10^6 \\ \begin{vmatrix} J_{3\alpha} & J_{3\beta} \\ J_{1\alpha} & J_{1\beta} \end{vmatrix} \approx -7.7710 \times 10^8 \end{cases} \tag{23}$$

So this singularity is removed. For the same reason, all the singularities in the workspace can be eliminated by using the redundant drive method.

Notice that the redundant drive method can only avoid the forward kinematics singularity. In fact, a redundant kinematics sub-chain with or without an actuator can both bring more inverse kinematics singularities (boundary). In equation (39), let

$$\begin{bmatrix} J_{1\theta 1} & 0 & 0 \\ 0 & J_{2\theta 2} & 0 \\ 0 & 0 & J_{3\theta 3} \end{bmatrix} = 0 \tag{24}$$

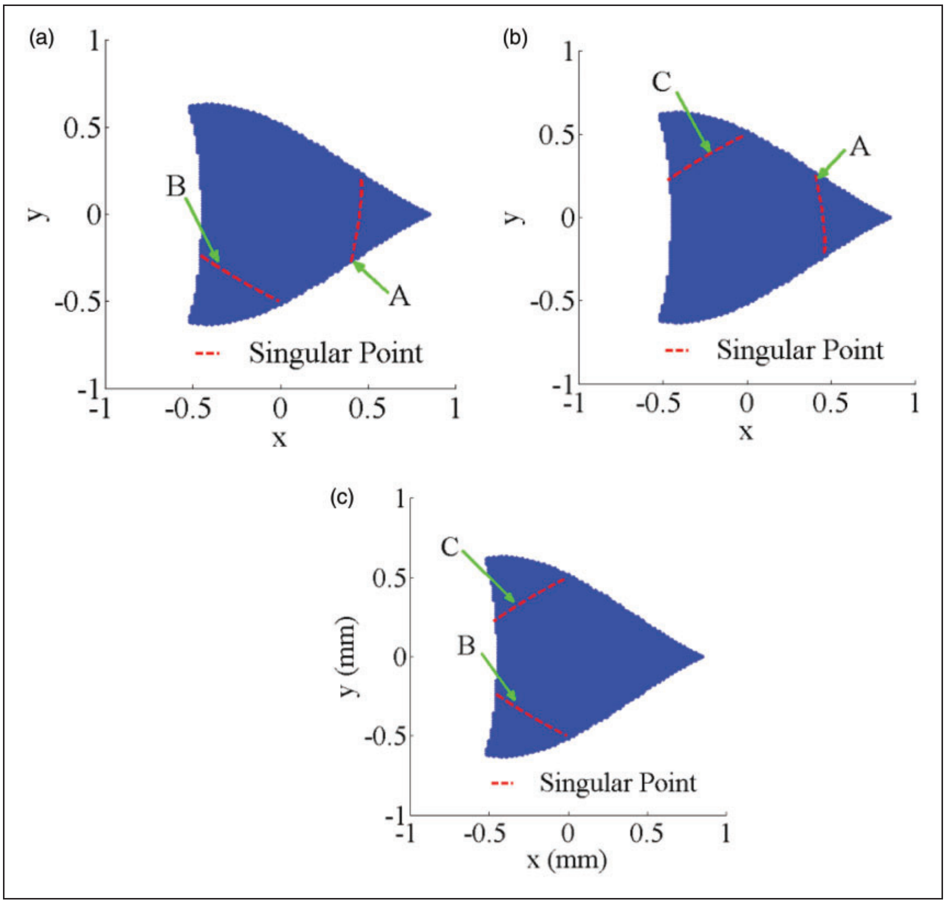

Figure 10. Orientation workspace with singularities driven by two arms. (a) Driven by arm1 and arm2 (b) Driven by arm1 and arm3 (c) Driven by arm2 and arm3.

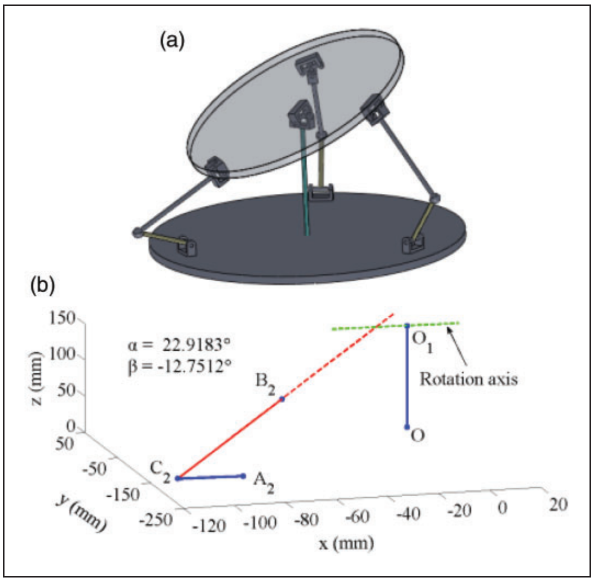

Figure 11. Singular configuration at $\alpha = 22.9183^{\circ}$, $\beta = -12.7512^{\circ}$. (a) Mechanism configuration (b) Geometric representation.

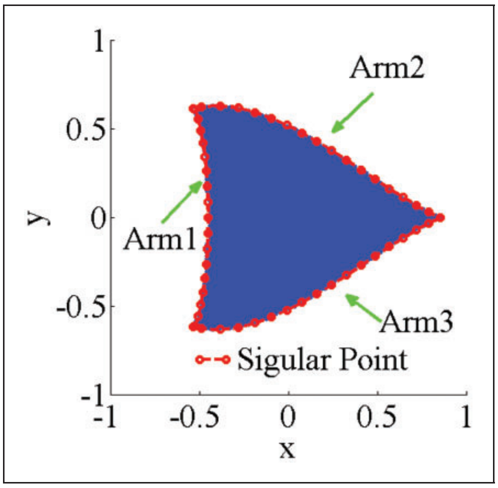

Figure 12. Orientation workspace with inverse kinematics singularities.

which means $J_{i\theta i} = 0$. Accordingly, the workspace with these singular configurations is shown in Figure 12.

In Figure 12, the dashed lines are the inverse kinematics singularities. As expected, they are the boundary lines. It is a way to determine the scope of the workspace exactly. If the parameters in Table 1 are modified as shown in Table 2, a platform with a larger orientation workspace (even can cover a whole sphere) also can be designed. However, by giving the above smaller workspace example, the characters of the mechanism should be presented more clearly.

Table 2. Modified parameters (*mm*).

R	r	h	l_1	l_2
166	106	140	120	200

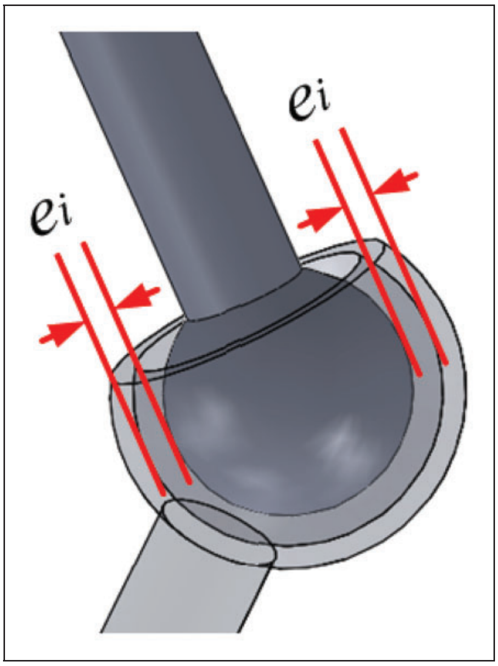

Figure 13. Spherical joint clearance.

Orientation error analysis

In pointing mechanism applications, the accuracy is of the utmost importance. Some previous works studied the accuracy of parallel mechanisms.[28–31] An error prediction model for overconstrained or non-overconstrained parallel mechanism was proposed.[32] Chang and Tsai[33] introduced a redundant drive method to control the backlash of a gear-coupled robotic mechanism. In this section, besides the analysis of the error caused by joint clearances, the error elimination by using redundant drive method is discussed.

For the presented mechanism, the analysis and manufacture of the spherical joints are the most complicated, so it is reasonable to assume each spherical joint has a joint clearance. As is shown in Figure 13, e_i means the clearance of the ith arm.

The clearances bring the errors of α and β directly, and then they can be mapped to the orientation error which is obtained from equation (16) as

$$\Delta \boldsymbol{P} = \frac{\partial \boldsymbol{P}}{\partial \alpha}\Delta\alpha + \frac{\partial \boldsymbol{P}}{\partial \beta}\Delta\beta \approx \begin{bmatrix} \Delta\beta c\beta \\ -\Delta\alpha c\alpha c\beta + \Delta\beta s\alpha s\beta \\ -\Delta\alpha s\alpha c\beta - \Delta\beta c\alpha s\beta \end{bmatrix} \tag{25}$$

The error can be measured by the modulus of equation (25) as

$$\|\Delta \boldsymbol{P}\| = \sqrt{(\Delta\alpha c\beta)^2 + (\Delta\beta)^2} \tag{26}$$

To get $\Delta\alpha$ and $\Delta\beta$, the clearance of each spherical joint can be seen as an error of l_2. So the length of B_iC_i will be $l_2 \pm \Delta l_2$, where $-e_i \leqslant \Delta l_2 \leqslant e_i$. Since the forward kinematics is a time consuming task and it is difficult to determine the maximum error, a new method should be proposed. If all the active arms move to their nominal angles, variables α, β, and l_2 may have errors. Assuming the nominal values of α and β are α_0 and β_0, respectively, using Taylor's theorem we get

$$\begin{aligned} &F_i(\alpha_0 + \Delta\alpha, \beta_0 + \Delta\beta, l_2 + \Delta l_i) \\ &\approx F_i(\alpha_0, \beta_0, l_2) + \frac{\partial F_i}{\partial \alpha}\Delta\alpha + \frac{\partial F_i}{\partial \beta}\Delta\beta + \frac{\partial F_i}{\partial l_2}\Delta l_i \end{aligned} \tag{27}$$

According to equation (5)

$$\begin{cases} F_i(\alpha_0 + \Delta\alpha, \beta_0 + \Delta\beta, l_2 + \Delta l_i) = 0 \\ F_i(\alpha_0, \beta_0, l_2) = 0 \end{cases} \tag{28}$$

Since the clearances are always small, the following equation will be precise enough

$$J_{i\alpha}\Delta\alpha + J_{i\beta}\Delta\beta - 2l_2\Delta l_i = 0 \tag{29}$$

First, let the mechanism be driven by arms 1 and 2 only, while arm3 is passive. Solving the equations (not in singularity configuration), we get

$$\begin{cases} \Delta\alpha = \dfrac{2l_2\left(J_{2\beta}\Delta l_1 - J_{1\beta}\Delta l_2\right)}{J_{1\alpha}J_{2\beta} - J_{1\beta}J_{2\alpha}} \\ \Delta\beta = \dfrac{2l_2(J_{1\alpha}\Delta l_2 - J_{2\alpha}\Delta l_1)}{J_{1\alpha}J_{2\beta} - J_{1\beta}J_{2\alpha}} \end{cases} \tag{30}$$

Substituting it to equation (26), the maximum error is

$$\|\Delta \boldsymbol{P}_{\max}\| = \frac{2l_2\sqrt{\begin{aligned} &\left(J_{2\alpha}^2 + J_{2\beta}^2 c^2\beta\right)\Delta l_1^2 \\ &+ \left(J_{1\alpha}^2 + J_{1\beta}^2 c^2\beta\right)\Delta l_2^2 \\ &+ 2\left|\left(J_{1\alpha}J_{2\alpha} + J_{1\beta}J_{2\beta}c^2\beta\right)\Delta l_1\Delta l_2\right| \end{aligned}}}{\left|J_{1\alpha}J_{2\beta} - J_{1\beta}J_{2\alpha}\right|} \tag{31}$$

From the result, it can be seen that $\Delta \boldsymbol{P}$ reaches its peak $\Delta \boldsymbol{P}_{\max}$ when $|\Delta l_1|$ and $|\Delta l_2|$ both get their maximum values. The sign selection of the term $\Delta l_1 \Delta l_2$ depends on the sign of the terms $J_{1\alpha}J_{2\alpha} + J_{1\beta}J_{2\beta}c^2\beta$. Assume $e_i = 0.1$ ($i = 1, 2, 3$), structure parameters are as shown in Table 1, and α, β [$-15°$, $15°$], the calculation result of the errors is plotted in Figure 14.

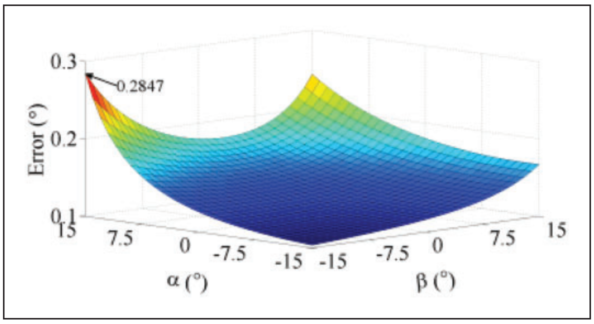

Figure 14. Maximum orientation errors when actuated by arm1 and arm2.

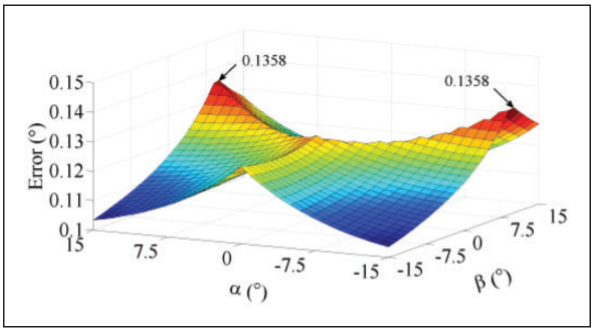

Figure 15. Maximum orientation errors when redundantly actuated.

Table 3. All possible sign sets for the three arms.

	Arm1	Arm2	Arm3
1	+	+	+
	−	−	−
2	+	+	−
	−	−	+
3	+	−	+
	−	+	−
4	+	−	−
	−	+	+

In the same way, the errors of the mechanism driven by any other two sub-chain arms can be obtained. If the platform is redundantly actuated, the error analysis is a little difficult. There are three non-redundant driven situations, but their signs of Δl_i are probably not in agreement. Taking the calculation of $||\Delta \boldsymbol{P}_{\max}||$ in a specific position as an example, if the mechanism is driven by arm1 and arm2, assuming the signs of Δl_1 and Δl_2 are both +; if the mechanism is driven by arm2 and arm3, assuming the signs of Δl_2 and Δl_3 are both +, too; while if the mechanism is driven by arm1 and arm3, assuming the signs of Δl_1 and Δl_3 are + and −, respectively. Then the two signs of Δl_3 are not in agreement, so the redundant error is not simply the minimum of the three situations. The redundant error analysis of the redundant drive mechanism should be as follows. All possible sign sets of the three arms are listed in Table 3.

There are four groups in Table 3, and the two sign sets of each group have the same maximum error. For each group, there are three non-redundant errors depend on the different selection of active arms. The minimum of them is the value of this group as the redundant error, and the overall redundant actuated error is the maximum of the four group values. Accordingly, the redundant drive errors are calculated as shown in Figure 15.

Comparing with Figure 14, the overall maximum error decreases from 0.2847° to 0.1358°. Generally, it can be seen that the errors are obviously reduced. The result corresponds to the intuition and gives a quantitative answer to the proposed accuracy problem. In fact, the errors can be totally eliminated by adjusting the displacements of the three redundant drive arms. Since α and β are both in their nominal values, according to the above error analysis

$$J_{i\theta i}\Delta\theta_i - 2l_2\Delta l_i = 0 \tag{32}$$

so

$$|\Delta\theta_i| = \left|\frac{2l_2\Delta l_i}{J_{i\theta i}}\right| \tag{33}$$

For the given example, to eliminate the orientation errors, the absolute displacement values of the three arms should be adjusted as shown in Figure 16.

The three arms should be in an antagonistic configuration, so the adjustment direction of each arm can be determined quickly.

Conclusions

A redundantly actuated 2-DOF rotational parallel mechanism for use as an antenna pointing device has been proposed in this paper. The parallel platform can be driven by three identical arms with rotary actuators fixed on the base. Both the forward and inverse kinematics analyses of the mechanism have been investigated, including the study of the differential kinematics. There are two possible solutions of the inverse kinematics and at most four possible solutions of the forward kinematics. The orientation workspace of the device is given which is an axis-symmetric shape. The kinematic singularities in the workspace have been investigated according to the Jacobian matrix, and the geometry representation of the forward singularity is explained. The non-redundant drive forward singularities are caused by the arms and can be expressed as unbroken lines in the orientation workspace. It is clearly demonstrated that the singularities can be reduced or eliminated by using redundant drive method. The maximum orientation errors caused by the spherical joint clearances in redundant and non-redundant drive situations have

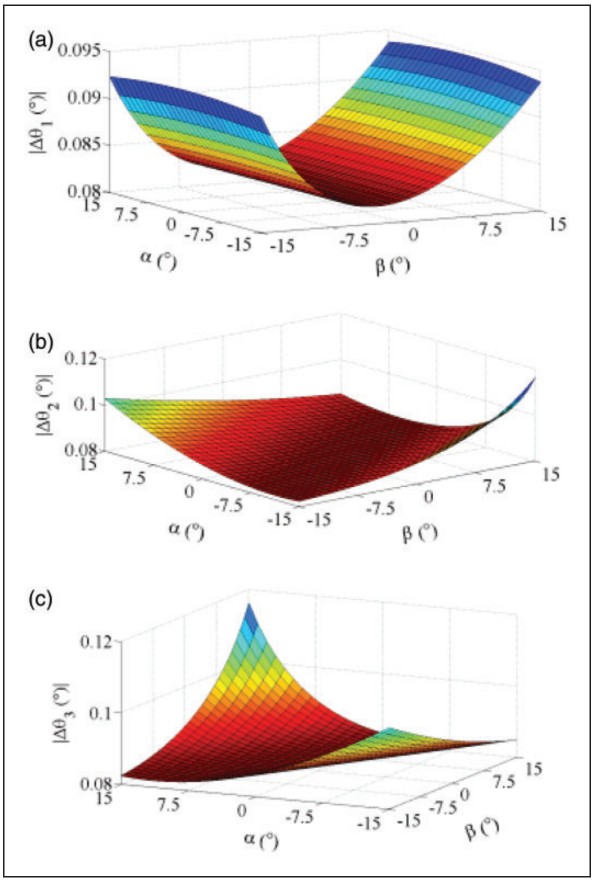

Figure 16. Absolute displacement values of the three arms should be adjusted. (a) Arm1, (b)Arm2, (c) Arm3.

been obtained. In addition, the error elimination method of adjusting displacements of the three active arms has been proposed. All of these investigations are explained and verified by numerical simulations, which show the redundant drive method is an effective way to avoid singularity configuration and to improve the pointing accuracy.

Declaration of Conflicting Interests

The author(s) declared no potential conflicts of interest with respect to the research, authorship, and/or publication of this article.

Funding

The author(s) disclosed receipt of the following financial support for the research, authorship, and/or publication of this article: The authors are grateful to the National Natural Science Foundation of China (Grant Nos. 51125020, 51105013), the Innovation Foundation of BUAA for PhD Graduates and the China Scholarship Council (Grant No. 201306020091) for the financial support of this work.

References

1. Dunlop GR and Jones TP. Position analysis of a two DOF parallel mechanism – the Canterbury tracker. *Mech Mach Theory* 1999; 34(4): 599–614.
2. Sofka J, et al. Omni-Wrist III – a new generation of pointing devices. Part I. Laser beam steering devices – mathematical modeling. *IEEE Transac Aerospace Electron Syst* 2006; 42: 718–25.
3. Carricato M and Parenti-Castelli V. A novel fully decoupled two-degrees-of-freedom parallel wrist. *Int J Robot Res* 2004; 23(6): 661–667.
4. Gogu G. Fully-isotropic over-constrained parallel wrists with two degrees of freedom. In: *2005 IEEE international conference on robotics and automation,* 18–22 April 2005. Barcelona, Spain: Institute of Electrical and Electronics Engineers Inc.
5. Jianyong Z, et al. Workspace and kinematics analysis of a 2-DOF Decoupled spherical parallel mechanism. In: *15th international conference on mechatronics and machine vision in practice,* Auckland, New Zealand, 2–4 December 2008. Availble at: http://ieeexplore.ieee.org/xpl/articleDetails.jsp?arnumber=4749567.
6. Yu J, et al. Mobility and singularity analysis of a class of two degrees of freedom rotational parallel mechanisms using a visual graphic approach. *J Mech Robot* 2012; 4: 041006-1–041006-10. Available at: http://mechanismsrobotics.asmedigitalcollection.asme.org/article.aspx?articleid=1484802.
7. Merriam EG, et al. Monolithic 2 DOF fully compliant space pointing mechanism. *Mech Sci* 2013; 4: 381–390.
8. Palpacelli MC, Palmieri G and Callegari M. A redundantly actuated 2-degrees-of-freedom mini pointing device. *J Mech Robot* 2012; 4: 031012-1–031012-10. Available at: http://mechanismsrobotics.asmedigitalcollection.asme.org/article.aspx?articleid=1484783.
9. Shao B, et al. Modeling and design of a novel precision tilt positioning mechanism for inter-satellite optical communication. *Smart Mater Struct* 2009; 18: 035009-1–035009-6. Available at: http://iopscience.iop.org/article/10.1088/0964-1726/18/3/035009/meta.
10. Saglia JA, et al. A high-performance redundantly actuated parallel mechanism for ankle rehabilitation. *Int J Robot Res* 2009; 28: 1216–1227.
11. Wang C, et al. Design and kinematical performance analysis of a 3-RUS/RRR redundantly actuated parallel mechanism for ankle rehabilitation. *J Mech Robot* 2013; 5: 041003-1–041003-11. Available at: http://mechanismsrobotics.asmedigitalcollection.asme.org/article.aspx?articleid=1714581.
12. Leguay-Durand S and Reboulet C. Optimal design of a redundant spherical parallel manipulator. *Robotica* 1997; 15: 399–405.
13. Wiitala JM and Stanišić MM. Design of an overconstrained and dextrous spherical wrist. *J Mech Des* 1998; 122: 347–353.
14. Enferadi J and Tootoonchi AA. A novel spherical parallel manipulator: forward position problem, singularity analysis, and isotropy design. *Robotica* 2009; 27: 663–676.
15. Di Gregorio R. A new family of spherical parallel manipulators. *Robotica* 2002; 20: 353–358.
16. Lenarcic J and Stanisic M. A humanoid shoulder complex and the humeral pointing kinematics. *IEEE Trans Robot Automat* 2003; 19: 499–506.
17. Lenarcic J, Stanisic MM and Parenti-Castelli V. Kinematic design of a humanoid robotic shoulder complex. In: *ICRA 2000 IEEE international conference on*

robotics and automation, 24–28 April 2000. San Francisco, CA, USA: IEEE, pp. 27–32.
18. De Sapio V, Holzbaur K and Khatib O. The control of kinematically constrained shoulder complexes: physiological and humanoid examples. In: *IEEE international conference on Robotics and automation*, Orlando, Florida, USA, 15–19 May 2006, pp. 2952–2959.
19. Seok-Hee L, et al. Kinematic analysis and implementation of a spherical 3-degree-of-freedom parallel mechanism. In: *2005 IEEE/RSJ international conference on intelligent robots and systems,* 2–6 August 2005. Piscataway, NJ, USA: IEEE, pp. 972–977. Available at: http://ieeexplore.ieee.org/xpl/freeabs_all.jsp?arnumber=1545080.
20. Gosselin CM and Hamel JF. The agile eye: a high-performance three-degree-of-freedom camera-orienting device. In: *Proceedings of the 1994 IEEE international conference on robotics and automation*, 8–13 May 1994. Los Alamitos, CA, USA: IEEE Comput. Soc. Press, pp. 781–786. Available at: http://ieeexplore.ieee.org/xpl/articleDetails.jsp?arnumber=351393.
21. Parenti-Castelli V and Innocenti C. Forward displacement analysis of parallel mechanisms. Closed form solution of PRR-3S and PPR-3S structures. *J Mech Des Trans ASME* 1992; 114: 68–73.
22. Bonev IA and Ryu J. A new approach to orientation workspace analysis of 6-DOF parallel manipulators. *Mech Mach Theory* 2001; 36: 15–28.
23. Merlet JP. Singular configurations of parallel manipulators and Grassmann geometry. *Int J Robot Res* 1989; 8(5): 45–56.
24. Pendar H, Mahnama M and Zohoor H. Singularity analysis of parallel manipulators using constraint plane method. *Mech Mach Theory* 2011; 46: 33–43.
25. Gosselin C and Angeles J. Singularity analysis of closed-loop kinematic chains. *IEEE Trans Robot Automat* 1990; 6: 281–290.
26. Ben-Horin P and Shoham M. Singularity condition of six-degree-of-freedom three-legged parallel robots based on grassmann-cayley algebra. *IEEE Trans Robot* 2006; 22: 577–590.
27. Jongwon K, et al. Design and analysis of a redundantly actuated parallel mechanism for rapid machining. *IEEE Trans Robot Automat* 2001; 17: 423–434.
28. Chebbi AH, Affi Z and Romdhane L. Prediction of the pose errors produced by joints clearance for a 3-UPU parallel robot. *Mech Mach Theory* 2009; 44: 1768–1783.
29. Briot S and Bonev IA. Accuracy analysis of 3T1R fully-parallel robots. *Mech Mach Theory* 2010; 45: 695–706.
30. Frisoli A, et al. A new screw theory method for the estimation of position accuracy in spatial parallel manipulators with revolute joint clearances. *Mech Mach Theory* 2011; 46: 1929–1949.
31. Merlet JP. Jacobian, manipulability, condition number, and accuracy of parallel robots. *J Mech Des Trans ASME* 2006; 128: 199–206.
32. Meng J, Zhang D and Li Z. Accuracy analysis of parallel manipulators with joint clearance. *J Mech Des Trans ASME* 2009; 131: 0110131–0110139.
33. Chang S-L and Tsai L-W. On the redundant-drive backlash-free robotic mechanisms. *J Mech Des* 1993; 115: 247–254.

Appendix

Notation

e	joint error
h	height of the central strut
J_i	Jacobian coefficient
l_1	length of the lower arm
l_2	length of the upper arm
p_{ij}	the corresponding dimensional parameters
$\boldsymbol{P}$	pointing orientation
r	radius of the moving platform
R	radius of the base
$\mathbf{R}_x$	rotation matrix about x axis
$\mathbf{R}_{y1}$	rotation matrix about y_1 axis
α,β	pointing angles